

# DELAY-INDUCED PATTERNS IN A TWO-DIMENSIONAL LATTICE OF COUPLED OSCILLATORS

MARKUS KANTNER\*, SERHIY YANCHUK†, AND ECKEHARD SCHÖLL‡

**Abstract.** We show how a variety of stable spatio-temporal periodic patterns can be created in 2D-lattices of coupled oscillators with non-homogeneous coupling delays. A “hybrid dispersion relation” is introduced, which allows studying the stability of time-periodic patterns analytically in the limit of large delay. The results are illustrated using the FitzHugh-Nagumo coupled neurons as well as coupled limit cycle (Stuart-Landau) oscillators.

**Key words.** time delay, patterns, FitzHugh-Nagumo neurons, lattices, componentwise timeshift-transformation

**AMS subject classifications.** 34K13, 34K18, 34K20, 34K35, 34K60, 37L60, 37N25, 37N35, 93C23

**1. Introduction.** Coupled dynamical systems with time delays arise in various applications including semiconductor lasers [14, 23, 32, 37], electronic circuits [29], optoelectronic oscillators [36], neuronal networks [16, 33, 3], gene regulation networks [35], socio-economic systems [34, 25] and many others [10, 12, 44, 18, 13, 17]. Understanding the dynamics in such systems is a challenging task. Even a single oscillator with time delayed feedback exhibits phenomena, which are not expected in this class of systems, such as Eckhaus instability [38], coarsening [15], or chimera state [19]. Some of them, like low frequency fluctuations in laser systems with optical feedback are still to be understood [27]. The situation is even more complicated when several systems are interacting with non-identical delays. In this case, somewhat more is known about some specific coupling configurations, e.g. ring [28, 42, 4, 1], and less on more complex coupling schemes [16, 22, 8, 7, 2]. Recently, it has been shown that a ring of delay coupled systems possesses a rich variety of stable spatiotemporal patterns [28, 42]. For the neuronal models in particular, this implies the existence of a variety of spiking patterns induced by the delayed synaptic connections.

Here we present a system with time delayed couplings, which is capable of producing a variety of stable two-dimensional spatio-temporal patterns. More specifically, we show that a 2D regular set of dynamical systems  $\mathbf{u}_{m,n}(t)$  (neuronal models can be used) may exhibit a stable periodic behavior (periodic spiking) such that the oscillator  $\mathbf{u}_{m,n}(t)$  reaches its maximum (spikes) at a time  $\eta_{m,n}$ , which can be practically arbitrary chosen within the period. For this, time delays should be selected accordingly to some given simple rule. As particular cases, the synchronous, cluster, or splay states can be realized.

Our work is a generalization of the previous results on the ring [28, 42], extending them to the two-dimensional case. However, the analysis, which we have to employ has important differences. In particular, the combination of the spatial structure of the system (spatial coordinates  $m$  and  $n$ ) and temporal delays required the introduction of a so called “hybrid dispersion relation” for the investigation of the stability of

\*Weierstrass Institute for Applied Analysis and Stochastics, Mohrenstr. 39, 10117 Berlin, Germany (kantner@wias-berlin.de),

†Humboldt University of Berlin, Institute of Mathematics, Unter den Linden 6, 10099 Berlin, Germany (yanchuk@math.hu-berlin.de),

‡Technical University of Berlin, Institute of Theoretical Physics, Hardenbergstr. 36, 10623 Berlin, Germany (schoell@physik.tu-berlin.de).

stationary state and nonlinear plane waves in the homogeneous system. Roughly speaking, this hybrid dispersion relation is a synthesis of the dispersion relation from the pattern formation theory in spatially extended systems [6, 5] and the pseudo-continuous spectrum developed for purely temporal delay systems [38, 20, 39].

We believe that such a higher-dimensional extension allows to speculate about the possibility of employing such systems for generating or saving visual patterns, and can be probably of use for information processing purposes. Small arrays of delay-coupled optoelectronic oscillators have indeed already been realized experimentally [36]. Similarly, autonomous Boolean networks of electronic logic gates have been demonstrated as versatile tools for the realizations of various space-time patterns [30]. Moreover, our analysis provides another evidence that the delays in coupled systems can play a constructive functional role.

More specifically, we consider a lattice of  $M \times N$  delay-coupled systems (delay differential equations) of the form

$$(1.1) \quad \frac{d}{dt} \mathbf{u}_{m,n}(t) = \mathbf{F} \left( \mathbf{u}_{m,n}(t), \mathbf{u}_{m-1,n}(t - \tau_{m,n}^\downarrow) + \mathbf{u}_{m,n-1}(t - \tau_{m,n}^\rightarrow) \right),$$

$$m = 1, \dots, M; \quad n = 1, \dots, N,$$

where  $\mathbf{F} : \mathbb{R}^d \times \mathbb{R}^d \rightarrow \mathbb{R}^d$  is a nonlinear function determining the dynamics of  $\mathbf{u}_{m,n} \in \mathbb{R}^d$  in the lattice. The indices  $m$  and  $n$  determine the position of the node, see Fig. 1.1. We assume periodic boundary conditions  $\mathbf{u}_{M+1,n} \equiv \mathbf{u}_{1,n}$  and  $\mathbf{u}_{m,N+1} \equiv \mathbf{u}_{m,1}$  such that the system has translation invariance. Time delays  $\tau_{m,n}^\downarrow$  and  $\tau_{m,n}^\rightarrow$  denote the connection delays between the corresponding nodes. Since each node has two incoming connections, the arrows  $\downarrow$  and  $\rightarrow$  correspond to the coupling from the node located above, respectively left, see Fig. 1.1. Here we restrict the analysis to two systems: Stuart-Landau (SL) oscillators as a simplest dynamical system exhibiting limit cycle behavior and FitzHugh-Nagumo (FHN) systems as a representative of conductance based, excitable neuronal models [11, 24]. While the first model allows for a deeper analytical insight, the second one can be studied mainly numerically and shows similar qualitative results.

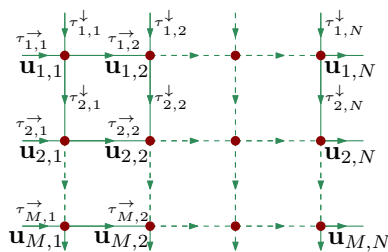


FIG. 1.1. *Coupling scheme. The dynamics of each node  $\mathbf{u}_{m,n}(t)$  is described by system (1.1). Each coupling connection possesses a delay  $\tau_{m,n}^\downarrow$  or  $\tau_{m,n}^\rightarrow$ . All edges are unidirectional.*

An example of a stable spatio-temporal pattern in a lattice of  $100 \times 150$  FHN neurons with non-homogeneous delays, the “Mona Lisa”-pattern is shown in Figure 1.2. Each frame corresponds to a snapshot at a fixed time  $t$  and the different level of gray at a point  $(m, n)$  corresponds to the value of the voltage component of  $\mathbf{u}_{m,n}(t)$  at this time  $t$ . More details on how such patterns can be created are given in the following sections, especially in Sec. 4.

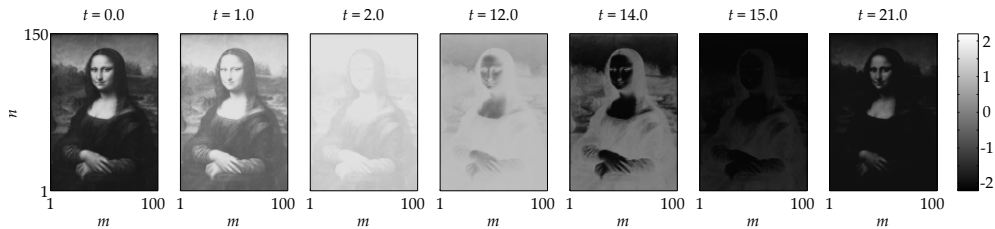


FIG. 1.2. Snapshots of the spatio-temporal behavior in a system of  $100 \times 150$  identical FHN neurons Eq. (3.1) with appropriately adjusted time delays  $\tau_{m,n}^\downarrow$  and  $\tau_{m,n}^\uparrow$ . At each grid point with the coordinate  $(m, n)$ , the level of gray (see colorbar) corresponds to the membrane voltage  $v_{m,n}(t)$  at this time moment. The pattern reappears periodically with a time period  $T = 21.95$ . More details are given in Sec. 4.

The structure of the remaining part of the paper is as follows: In Sec. 2 we consider SL systems with homogeneous time delays  $\tau_{m,n}^\rightarrow = \tau_{m,n}^\downarrow = \tau$ . We investigate the stability of the homogeneous steady state as well as various plane wave solutions in the system. The number of stable plane wave solutions is shown to increase with the delay. Further in Sec. 3 similar results are obtained for the FHN systems. Section 4 considers the case when the delays are not identical. In this case it is shown how a variety of spatiotemporal patterns can be created by varying the coupling delays. Finally, additional illustrative examples are presented in Sec. 4.2.

**2. Stuart-Landau oscillators with homogeneous coupling delays.** In this section we start with a lattice of SL oscillators with homogeneous delays  $\tau_{m,n}^\rightarrow = \tau_{m,n}^\downarrow = \tau$  as a model for the local dynamics:

$$(2.1) \quad \frac{d}{dt} z_{m,n}(t) = (\alpha + i\beta)z_{m,n}(t) - z_{m,n}(t)|z_{m,n}(t)|^2 + \frac{C}{2}(z_{m-1,n}(t-\tau) + z_{m,n-1}(t-\tau)).$$

The variables  $z_{m,n}$  are complex-valued. The parameter  $\alpha$  controls the local dynamics without coupling, i.e. a stable steady state exists for  $\alpha < 0$  and a stable limit cycle for  $\alpha > 0$ ;  $\beta$  is the frequency of this limit cycle. The coupling strength is determined by  $C > 0$ .

In this section we study the bifurcation scenario, which is associated with the destabilization of the homogeneous steady state  $z = 0$  and the appearance of various plane waves. Many aspects of this scenario can be studied analytically due to the  $S^1$  equivariance of the system:  $\mathbf{F}(e^{i\nu}\cdot, e^{i\nu}\cdot) = e^{i\nu}\mathbf{F}(\cdot, \cdot)$  for any real  $\nu$ . At some places we will assume additionally that the delay  $\tau$  is large comparing to the timescale of the system (we will mention it each time explicitly), which simplifies analytical calculations.

## 2.1. Stability and bifurcations of homogeneous stationary state.

**2.1.1. Characteristic equation and its solutions.** System (2.1) has a homogeneous steady state  $z_{m,n} \equiv 0$ . Let us investigate stability of this stationary state. Linearizing the equation of motion (2.1) around  $z_{m,n} = 0$  yields the following equation for the evolution of small perturbations  $\delta z_{m,n}(t)$ :

$$\frac{d}{dt} \delta z_{m,n}(t) = (\alpha + i\beta)\delta z_{m,n}(t) + \frac{C}{2}(\delta z_{m-1,n}(t-\tau) + \delta z_{m,n-1}(t-\tau)).$$

This equation can be diagonalized by a spatial discrete Fourier-transformation

$$\delta\tilde{z}_{k_1, k_2} = \sum_{m=1}^M \sum_{n=1}^N e^{ik_1 m + ik_2 n} \delta z_{m, n},$$

where the wavevector  $\mathbf{k} = (k_1, k_2)^T$  admits the following discrete values:

$$(2.2) \quad (k_1, k_2)^T = 2\pi \left( \frac{l}{M}, \frac{j}{N} \right)^T, \quad l = 1, \dots, M, \quad j = 1, \dots, N.$$

We obtain

$$(2.3) \quad \frac{d}{dt} \delta\tilde{z}_{k_1, k_2}(t) = (\alpha + i\beta) \delta\tilde{z}_{k_1, k_2}(t) + \frac{C}{2} (e^{ik_1} + e^{ik_2}) \delta\tilde{z}_{k_1, k_2}(t - \tau).$$

Since the equation for the Fourier modes is uncoupled, one can drop the indices  $k_1$  and  $k_2$  for simplicity and introduce the notations

$$(2.4) \quad k_{\pm} = \frac{1}{2} (k_1 \pm k_2),$$

which is just a rotation of coordinates in the Fourier space. Note that  $k_{\pm}$  admits discrete values accordingly to (2.2). Then the system (2.3) can be rewritten as

$$\frac{d}{dt} \delta\tilde{z}(t) = (\alpha + i\beta) \delta\tilde{z}(t) + C e^{ik_+} \cos(k_-) \delta\tilde{z}(t - \tau).$$

Since the modes are decoupled in the Fourier space, the corresponding characteristic equation factorizes and reads

$$(2.5) \quad 0 = \prod_{\{(k_+, k_-)\}} (-\lambda + \alpha + i\beta + C \cos(k_-) e^{ik_+ - \lambda\tau}).$$

This is a transcendental equation in  $\lambda$ , which can be solved as

$$(2.6) \quad \lambda_j = \alpha + i\beta + \frac{1}{\tau} W_j \left( \tau C \cos(k_-) e^{ik_+ - (\alpha + i\beta)\tau} \right),$$

for all admitted pairs  $(k_+, k_-)$ , where  $j$  denotes the  $j$ th branch of the Lambert  $W$ -function. This formula can be used for studying the stability of the homogeneous state. In particular, if all eigenvalues  $\lambda_j$  have negative real parts for all possible wavevectors  $k_{\pm}$ , then the steady state is asymptotically stable.

**2.1.2. Large delay approximation.** A deeper understanding of the spectrum can be achieved for large delays using the asymptotic methods [20, 31, 13]. Accordingly to these results, the spectrum splits generically into two parts accordingly to the asymptotics for large delays. The first part is called the *strongly unstable spectrum* and the second part is the *pseudo-continuous spectrum*. The strong spectrum exists for  $\alpha > 0$  and consists of two complex conjugate, isolated roots which are close to  $\lambda_{S, \pm} = \alpha \pm i\beta$ . In such a case, the contribution of the term  $\frac{1}{\tau} W_j[\cdot]$  in (2.6) vanishes. In fact, the strong spectrum always converges to the unstable part of the spectrum of the system with omitted delayed terms [40, 39, 20], i.e.  $\frac{d}{dt} \delta\tilde{z}(t) = (\alpha + i\beta) \delta\tilde{z}(t)$  in this case. Besides the strong spectrum there are infinitely many more eigenvalues,

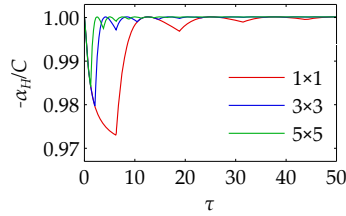


FIG. 2.1. Destabilization threshold of the homogeneous stationary state in lattices of coupled Stuart-Landau oscillators as a function of the coupling delay. The asymptotic result  $\alpha_H = -C$  is exact for vanishing and infinite delay. However, also for moderate delays the approximation sufficiently matches the numerical results.

accumulating on some curves in the complex plane as  $\tau \rightarrow \infty$ . These eigenvalues form the pseudo-continuous spectrum and can be found by substituting the ansatz  $\lambda = \frac{1}{\tau}\gamma(\Omega) + i\Omega$  in the characteristic equation (2.5). One obtains

$$i\Omega = \alpha + i\beta + C \cos(k_-) e^{ik_+} e^{-\gamma - i\Omega\tau},$$

where the small term  $\gamma/\tau$  has been neglected. It can be solved as

$$Y := e^{-\gamma} e^{i(k_+ - \Omega\tau)} = -\frac{\alpha + i(\beta - \Omega)}{C \cos(k_-)}$$

and finally for the curve  $\gamma(\Omega)$  we obtain

$$(2.7) \quad \gamma(\Omega) = -\frac{1}{2} \log |Y|^2 = -\frac{1}{2} \log \left( \frac{\alpha^2 + (\beta - \Omega)^2}{C^2 \cos^2(k_-)} \right).$$

Note that the spectrum is invariant with respect to complex conjugation. It is easy to see that the spatial mode  $k_- = 0$  corresponds to the maximal values of  $\gamma(\Omega)$ . Thus, the spatial modes with  $k_- = 0$  are most unstable. Moreover, it is easy to check that the leading value of  $\gamma$  is negative if  $|\alpha| > C$  and positive otherwise. This implies that the homogeneous steady state is asymptotically stable for  $\alpha < -C$  and unstable for  $\alpha > -C$  (we take also into account that there is a strongly unstable spectrum for  $\alpha > 0$ ). Hence, the destabilization takes place at  $\alpha = -C$  via Hopf bifurcation at the frequency  $\Omega \approx \beta$ . Here we should remark that our conclusions are rigorous for long enough delay  $\tau$ . In our case, however, the destabilization threshold is well approximated by this value already for moderate delays, see Fig. 2.1.

The illustration by the numerically computed eigenvalues is shown in Fig. 2.2 for the system of  $3 \times 3$  coupled SL oscillators for three cases: stable, critical, and unstable. One can observe also how multiple Hopf bifurcation may emerge after the destabilization. In the following section we discuss the plane waves arising in these Hopf bifurcations.

## 2.2. Nonlinear plane waves and their stability.

**2.2.1. Branches of plane wave solutions.** Because of the  $S^1$ -equivariance of the Stuart-Landau system (2.1), periodic solutions emerging from the homogeneous steady state via Hopf bifurcations have the following explicit form

$$(2.8) \quad z(t) = a e^{i\Omega t - ik_1 m - ik_2 n}.$$

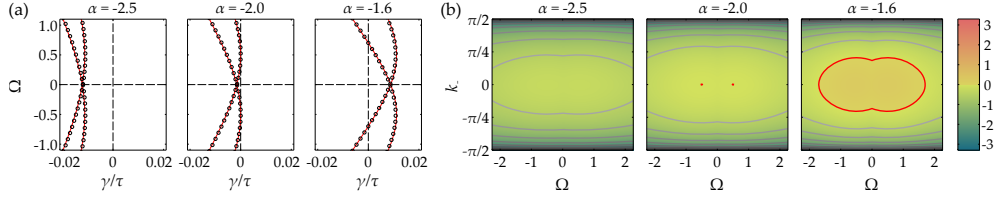


FIG. 2.2. (a) Destabilization of the zero steady state in  $3 \times 3$  lattice of delay coupled SL oscillators with  $C = 2$ ,  $\beta = 0.5$ , and  $\tau = 20$ . The plot shows numerically computed eigenvalues (solutions of Eq. (2.5)) and the continuous large delay approximation (2.7) by the red line. At  $\alpha = -2.5$  the stationary state is stable,  $\alpha = -2$  is the critical case, and for  $\alpha = -1.6$  an unstable steady state is shown. All eigenvalues accumulate along the curves  $\gamma(\Omega, k_-)$  given by Eq. (2.7) with maxima at  $\Omega = \pm\beta$ . (b) Destabilization of the stationary state in an infinitely large lattice, where  $k_-$  becomes a continuous parameter. The density plot shows the scaled real part of the eigenvalues  $\text{Re } \gamma = \lambda/\tau$ . The parameters are the same as on the left.

The amplitude  $a$ , frequency  $\Omega$ , and the wavevector  $\mathbf{k} = (k_1, k_2)^T$  of the periodic solutions satisfy the following relation

$$i\Omega = \alpha + i\beta - a^2 + e^{i(k_+ - \Omega\tau)} C \cos(k_-),$$

which is obtained by substituting (2.8) into (2.1). Here we recall that  $k_{\pm}$  is the wavevector in rotated coordinates (2.4). Taking real and imaginary parts, we obtain

$$(2.9a) \quad a^2 = \alpha + R \cos k_{\tau},$$

$$(2.9b) \quad \Omega = \beta + R \sin k_{\tau},$$

where we denote  $R := C \cos k_-$  and  $k_{\tau} := k_+ - \Omega\tau$ . By excluding  $k_{\tau}$  we obtain

$$(2.10) \quad (a^2 - \alpha)^2 + (\Omega - \beta)^2 = R^2.$$

Therefore all periodic solutions can be found on circles in the  $(a^2, \Omega)$ -parameter space as shown in Fig. 2.3. Equation (2.9b) is known as *Kepler's equation* and can be solved numerically with respect to  $\Omega$ . The number of solutions of (2.9b) matches the number of Hopf bifurcations and periodic solutions. All possible frequencies are confined to the interval  $-|R| + \beta \leq \Omega \leq |R| + \beta$ . The corresponding value for the parameter  $\alpha$ , at which Hopf bifurcation occurs, is then given by Eq. (2.9a) with  $a^2 = 0$ . For a system of the size  $N \times N$ , the number of Hopf bifurcations, or periodic solutions respectively, can be estimated by

$$\mathcal{N}_H \approx \begin{cases} \frac{2C\tau}{\pi} N \frac{1}{\sin(\frac{\pi}{2N})} & N \text{ even,} \\ \frac{2C\tau}{\pi} N \cot(\frac{\pi}{2N}) & N \text{ odd.} \end{cases}$$

In the case of large  $N$  the asymptotic number of solutions is given by

$$(2.11) \quad \mathcal{N}_H \sim \frac{4C\tau}{\pi^2} N^2.$$

Thus, in the case of large delay or lattice-size the number of solutions grows and any point on the circles (2.10) refers to a periodic solution, i.e. the circle disk is densely filled with points  $(a, \Omega)$  corresponding to the existing periodic solutions. Indeed, for an infinitely large lattice, the wavevector  $\mathbf{k}$  admits any values from  $\mathbb{R}^2$ . Therefore one obtains continuous parameters  $k_- \in (-\pi, \pi)$  and  $k_{\tau} = (k_+ - \Omega\tau) \in (0, 2\pi)$ , which parametrize all periodic solutions of Eq. (2.1).

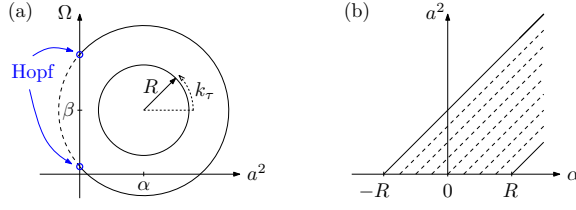


FIG. 2.3. (a) Frequency  $\Omega$  versus amplitude  $a$  of periodic solution (2.8). The admissible parameters are located on the circles with radii  $R$  [Eq. 2.3], except the parts with  $a^2 < 0$ . (b) Branches of periodic solutions emerge from the steady state within the interval  $\alpha \in [-|R|, |R|]$ .

**2.2.2. Stability of plane wave solutions.** The local asymptotic stability of plane wave solutions can be studied using the linearized equation for small perturbations  $\delta z_{m,n}(t)$ . In co-rotating coordinates  $\xi_{m,n}$  determined by

$$(2.12) \quad z_{m,n}(t) = e^{i(\Omega t - k_1 m - k_2 n)} u_{m,n}(t),$$

the plane wave is just the steady state  $u_{m,n} = a$ . Therefore, after changing the coordinates (2.12), substituting  $u_{m,n}(t) = a + \xi_{m,n}(t)$ , and linearizing the obtained equation in small perturbations  $\xi_{m,n}(t)$ , we obtain

$$(2.13) \quad \begin{aligned} \frac{d}{dt} \xi_{m,n}(t) &= (\alpha + i\beta - i\Omega - 2a^2) \xi_{m,n}(t) - a^2 \xi_{m,n}^*(t) + \\ &+ \frac{C}{2} e^{-i\Omega\tau} (e^{ik_1} \xi_{m-1,n}(t-\tau) + e^{ik_2} \xi_{m,n-1}(t-\tau)). \end{aligned}$$

The solutions of the obtained linear equation can be found by the ansatz

$$(2.14) \quad \xi_{m,n}(t) = b_1 e^{\lambda t - iq_1 m - iq_2 n} + b_2^* e^{\lambda^* t + iq_1 m + iq_2 n}.$$

The ansatz (2.14) can be obtained, e.g. by rewriting the system (2.13) in the real form, diagonalizing it with the discrete Fourier transform (similar to (2.3)), and noticing that the equations for the Fourier components  $\tilde{\xi}_{q_1, q_2}$  and  $\tilde{\xi}_{-q_1, -q_2}$  are complex conjugate, and hence, they have the same stability properties with the complex conjugate eigenvalues, see also [5]. After substituting (2.14) into (2.13), the coefficients at the two linearly independent functions  $e^{\lambda t - iq_1 m - iq_2 n}$  and  $e^{\lambda^* t + iq_1 m + iq_2 n}$  should be zero. This leads to the system of two linear equations for unknowns  $b_1$  and  $b_2$ :

$$\begin{aligned} \left[ \alpha + i\beta - i\Omega - \lambda - 2a^2 + \frac{C}{2} e^{-(\lambda + i\Omega)\tau} (e^{i(k_1 + q_1)} + e^{i(k_2 + q_2)}) \right] b_1 - a^2 b_2 &= 0, \\ -a^2 b_1 + \left[ \alpha - i\beta + i\Omega - \lambda - 2a^2 + \frac{C}{2} e^{-(\lambda - i\Omega)\tau} (e^{-i(k_1 - q_1)} + e^{-i(k_2 - q_2)}) \right] b_2 &= 0. \end{aligned}$$

This system has a nontrivial solution if the determinant of its matrix is zero. We arrive at the characteristic equation

$$(2.15) \quad \begin{aligned} \chi(\lambda, q_-, q_+) &= \lambda^2 + 2(a^2 + R \cos k_\tau) \lambda + R^2 + 2Ra^2 \cos k_\tau + R_+ R_- e^{-2\lambda\tau + 2iq_+ -} \\ &- \left[ (a^2 + R \cos k_\tau + \lambda) (R_+ e^{ik_\tau} + R_- e^{-ik_\tau}) - \right. \\ &\left. - iR \sin k_\tau (R_+ e^{ik_\tau} - R_- e^{-ik_\tau}) \right] e^{-\lambda\tau + iq_+}, \end{aligned}$$

where we additionally denote  $q_{\pm} := \frac{1}{2}(q_1 \pm q_2)$  and  $R_{\pm} := C \cos(k_- \pm q_-)$ . Now the obtained characteristic equation (2.15) determines the stability of a plane wave. Namely, for any plane wave, which is defined by the amplitude  $a$ , frequency  $\Omega$ , wave-vectors  $k_+$  and  $k_-$  (then also  $k_{\tau} = k_+ - \Omega\tau$  is given), the equation (2.15) determines the stability with respect to the perturbation mode with the spatial perturbations  $q_+$  and  $q_-$ . In particular, if for all  $q_+, q_- \in [0, 2\pi]$ , all the solutions  $\lambda$  of the characteristic equation (2.15) have negative real parts, then the plane wave is asymptotically stable. The symmetry-relation  $\chi^*(\lambda^*, q_-, -q_+; -k_{\tau}) = \chi(\lambda, q_-, q_+; k_{\tau})$  implies, that the stability properties of periodic solutions are invariant with respect to changing  $k_{\tau} \rightarrow -k_{\tau}$ . Notice that the obtained equation is a quasi-polynomial, which has generically infinitely many roots.

Although Eq. (2.15) can be studied numerically for each given set of parameters, an additional useful analytical insight in the properties of its solutions is possible under the assumption of large delay  $\tau$ . This is performed in the next section.

### 2.2.3. Stability of plane wave solutions: large delay approximation.

**Strong spectrum.** As it was discussed in Sec. 2.1.2, the strong spectrum involves only the instantaneous part of the dynamics. Therefore it does not depend on the spatial perturbation modes  $\mathbf{q}$  or the network-size, since all spatial effects induced by the coupling-structure are contained in the delayed terms. The reduced characteristic equation for the strong spectrum can be formally obtained by setting  $e^{-\lambda\tau} e^{iq_+} = 0$  in (2.5):

$$0 = \lambda^2 + 2(2a^2 - \alpha)\lambda + 2a^2(a^2 - \alpha) + R^2$$

Its solutions are

$$\lambda_{\pm} = \alpha - 2a^2 \pm \sqrt{a^4 + (a^2 - \alpha)^2 - R^2}.$$

Any of the solutions  $\lambda_{\pm}$  with positive real part belongs to the strong spectrum. Simple calculations show that there exists at least one strong eigenvalue with positive real part if

$$(2.16) \quad a^2 < a_S^2(\alpha; R) = \begin{cases} \alpha/2 & \text{for } -|R| \leq \alpha \leq \sqrt{2}|R| \\ \frac{1}{2}(\alpha + \sqrt{\alpha^2 - 2R^2}) & \text{for } \sqrt{2}|R| < \alpha, \end{cases}$$

i.e. if the amplitude of the plane wave is smaller than the one determined by the curve  $a_S(\alpha, R)$ . Moreover, when the inequality  $a^4 + (a^2 - \alpha)^2 - R^2 < 0$  is satisfied, there are two complex conjugate unstable eigenvalues  $\lambda_+ = \lambda_-^* \in \mathbb{C}$  with  $\text{Re } \lambda_{\pm} = \alpha - 2a^2$ . The bifurcation diagram in Fig. 2.5 illustrates the regions of strong instability of plane waves (dark gray regions, labeled with  $S$ ).

**Pseudo-continuous (weak) spectrum.** Besides the strong spectrum, there are infinitely many eigenvalues in the *weak* or *pseudo-continuous spectrum*. Similarly to Sec. 2.1.2, this spectrum can be found by substituting the ansatz

$$\lambda = \frac{\gamma(\omega)}{\tau} + i\omega$$

into the characteristic equation (2.15). In the limit of large delay, the terms of the order  $\mathcal{O}(1/\tau)$  can be neglected, resulting in the following equation

$$(2.17) \quad 0 = S(q_-)Y^2 - 2[A(\omega, q_-) + iB(\omega, q_-)]Y + D(\omega) + iE(\omega),$$

with  $Y := e^{-\lambda\tau} e^{iq_+}$ , and the real valued functions

$$\begin{aligned} S(q_-) &= R_+ R_- = C^2 \cos(k_- + q_-) \cos(k_- - q_-), \\ A(\omega, q_-) &= C \left( [R + a^2 \cos k_\tau] \cos k_- \cos q_- + \omega \sin k_\tau \sin k_- \sin q_- \right), \\ B(\omega, q_-) &= C \left( -a^2 \sin k_\tau \sin k_- \sin q_- + \omega \cos k_\tau \cos k_- \cos q_- \right), \\ D(\omega) &= R^2 - \omega^2 + 2Ra^2 \cos k_\tau, \\ E(\omega) &= 2\omega(a^2 + R \cos k_\tau). \end{aligned}$$

Note that the dependence on  $q_+$  in the obtained equation (2.17) is included only in  $Y$ . Solving the quadratic equation (2.17) with respect to  $Y$  leads to

$$Y_{\pm}(\omega, q_-) = \frac{1}{S(q_-)} \left( A(\omega, q_-) + iB(\omega, q_-) \pm \sqrt{\zeta(\omega, q_-)} \right),$$

with

$$\zeta(\omega, q_-) = A^2(\omega, q_-) - B^2(\omega, q_-) - S(q_-)D(\omega) + i[2A(\omega, q_-)B(\omega, q_-) - S(q_-)E(\omega)].$$

Since there are two solutions  $Y_{\pm}$ , one obtains two functions for the pseudo-continuous spectrum

$$\gamma_{\pm}(\omega, q_-) = -\log |Y_{\pm}| = -\frac{1}{2} \log (Y_{\pm} Y_{\pm}^*).$$

The spectrum possesses the following symmetries

$$(2.18) \quad Y_{\pm}(\omega, q_- + \pi) = -Y_{\mp}(\omega, q_-)$$

and

$$(2.19) \quad Y_{\pm}(-\omega, -q_-) = Y_{\pm}^*(\omega, q_-).$$

The first relation (2.18) implies that it is sufficient to consider only one of the two functions  $\gamma_{\pm}(\omega, q_-)$ , since they are related to each other by the shift  $q_- \rightarrow q_- + \pi$  as

$$(2.20) \quad \gamma_+(\omega, q_- + \pi) = \gamma_-(\omega, q_-).$$

This also indicates that the pseudo-continuous spectrum is twofold degenerate in the limit of  $M, N \rightarrow \infty$ . The second property (2.19) implies that the spectrum has the reflection-symmetry in the  $(\omega, q_-)$ -plane:

$$\gamma_{\pm}(-\omega, -q_-) = \gamma_{\pm}(\omega, q_-).$$

Note that in the special case  $k_- = 0$  the additional symmetry-relations  $Y_{\pm}(-\omega, q_-) = Y_{\pm}^*(\omega, q_-)$  and  $Y_{\pm}(\omega, -q_-) = Y_{\pm}(\omega, q_-)$  hold. Figure 2.4 illustrates the function  $\gamma_{\max}(\omega, q_-) = \max\{\gamma_+, \gamma_-\}$  for different values of  $k_-$  and  $k_\tau$ .

The eigenvalues  $\lambda$  are known as *characteristic exponents* or *Floquet-exponents* and are related to the *Floquet-multipliers* via  $\mu = e^{\lambda T} = \exp\left(\frac{2\pi\gamma}{\Omega\tau}\right) \exp\left(\frac{2\pi i\omega}{\Omega}\right)$ . As known from the Floquet-theory for periodic solutions, there is always one trivial multiplier  $\mu = 1$  or trivial exponent  $\lambda = 0$ , arising from the continuous symmetry with respect to timeshifts in autonomous systems (phase shift on the limit cycle). For a perturbation with  $\omega = 0$  and  $q_- = 0$  one obtains

$$Y_{\pm}(\omega = 0, q_- = 0) = 1 + \frac{a^2}{R} \cos k_\tau \left( 1 \pm \frac{\cos k_\tau}{|\cos k_\tau|} \right).$$

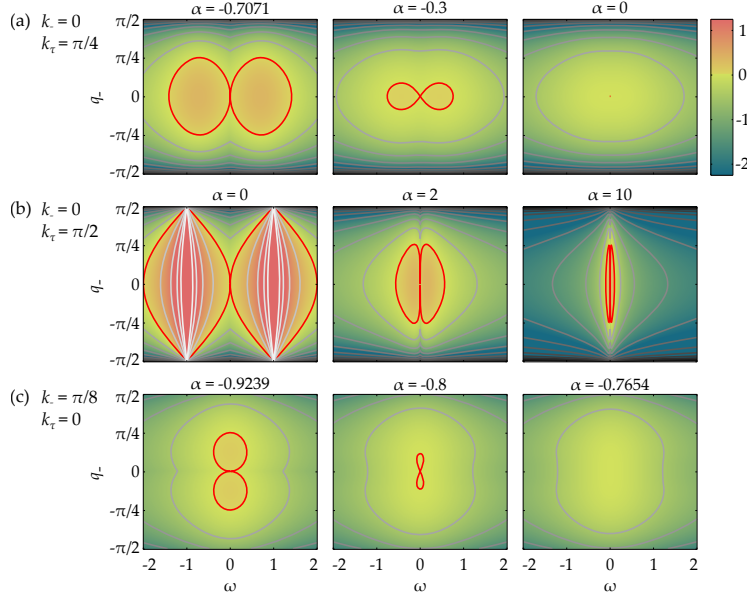


FIG. 2.4. Asymptotic continuous spectrum  $\gamma_{\max}(\omega, q_-)$  of periodic solutions for different values of  $k_-$  and  $k_+$ . The density plot shows the scaled real part of the leading eigenvalues. Note that this plot is similar to the Master stability function [13].

The corresponding characteristic exponent follows as

$$(2.21) \quad \begin{aligned} \gamma_+(\omega = 0, q_- = 0) &= \begin{cases} -\log\left(1 + 2\frac{a^2}{R} \cos k_\tau\right) < 0 & \text{for } \cos k_\tau \geq 0 \\ 0 & \text{for } \cos k_\tau < 0 \end{cases} \\ \gamma_-(\omega = 0, q_- = 0) &= \begin{cases} 0 & \text{for } \cos k_\tau \geq 0 \\ -\log\left(1 + 2\frac{a^2}{R} \cos k_\tau\right) > 0 & \text{for } \cos k_\tau < 0 \end{cases} \end{aligned}$$

Note that this property of the spectrum is not affected by the long delay approximation, since the approximation becomes exact at  $\gamma = 0$ . Apparently there are two parameter domains separated by  $\cos k_\tau = 0$ . Using (2.9a), one finds that this boundary corresponds to the curve  $a_U := \sqrt{\alpha}$ . Thus, all periodic solutions with the amplitudes smaller than  $a_U$  for a given  $\alpha$  are unstable due to a positive characteristic exponent with  $\omega = 0$ . According to [6] this instability is called a *uniform instability*. In order to determine the neutral stability curve, the following discussion is restricted to the regime with  $\cos k_\tau \geq 0$ . Since the relation (2.20) holds, we will focus the analysis on  $\gamma_-(\omega, q_-)$ .

The trivial multiplier always denotes a critical point of the pseudo-continuous spectrum at  $(\omega = 0, q_- = 0)$ , where the gradient vanishes:

$$\nabla \gamma_-|_{\omega=0, q_-=0} = \left( \frac{\partial}{\partial \omega}, \frac{\partial}{\partial q_-} \right) \gamma_- \Big|_{\omega=0, q_-=0} = 0.$$

This can be verified by a direct calculation. Therefore the point  $(\omega = 0, q_- = 0)$  is either an extremum or saddle of the pseudo-continuous spectrum. Analyzing the shape of the spectrum close to the trivial multiplier shows the appearance of the

*modulational instability* [5, 6], see also Fig. 2.4. For this, let us consider the second order approximation of  $\gamma_-$  at  $(\omega, q_-) = 0$ , involving the Hessian matrix

$$H = \left( \begin{array}{cc} \frac{\partial^2 \gamma_-}{\partial \omega^2} & \frac{\partial^2 \gamma_-}{\partial \omega \partial q_-} \\ \frac{\partial^2 \gamma_-}{\partial \omega \partial q_-} & \frac{\partial^2 \gamma_-}{\partial q_-^2} \end{array} \right) \Bigg|_{\omega=0, q_-=0}.$$

Direct calculation leads to the following expressions for the elements of the Hessian matrix

$$\begin{aligned} \frac{\partial^2 \gamma_-}{\partial \omega^2} \Bigg|_{\omega=0, q_-=0} &= \frac{1}{R^2 \cos^2 k_\tau} \left( \frac{R \sin^2 k_\tau}{a^2 \cos k_\tau} - 1 \right), \\ \frac{\partial^2 \gamma_-}{\partial q_-^2} \Bigg|_{\omega=0, q_-=0} &= -1 + \frac{R \tan^2 k_-}{a^2 \cos^3 k_\tau} + \tan^2 k_- \tan^2 k_\tau, \\ \frac{\partial^2 \gamma_-}{\partial \omega \partial q_-} \Bigg|_{\omega=0, q_-=0} &= \frac{\tan k_- \tan k_\tau}{a^2 \cos^2 k_\tau}. \end{aligned}$$

The curvature of the asymptotic continuous spectrum close to the trivial multiplier is directly related to the stability of the corresponding plane wave. If the surface is locally concave close to  $(\omega, q_-) = (0, 0)$ , then the Hessian is negative definite and the corresponding periodic orbit is stable (at least the part of the spectrum which is close to  $(\omega, q_-) = (0, 0)$ ). Otherwise, if the curvature is convex (Hessian is positive definite) or the origin is a saddle-point (Hessian is indefinite), the plane wave is unstable. The curvature is characterized by the real eigenvalues of the symmetric Hessian matrix. The analysis of the eigenvalues of the Hessian matrix leads to the following condition for the stability of the plane wave, which is the condition for the negativeness of the eigenvalues of  $H$ :

$$(\cos^2 k_\tau - \sin^2 k_-) (R \cos k_\tau + a^2) - R \cos k_\tau > 0.$$

Using the amplitude relation (2.9a), the bifurcation is described by a 3rd order polynomial in  $a^2$ :

$$(2.22) \quad 0 = a^6 - \frac{5}{2} \alpha a^4 + \left( 2\alpha^2 - \frac{R^2}{2} (1 + 2 \sin^2 k_-) \right) a^2 - \frac{\alpha^3}{2} + \frac{R^2 \alpha}{2} (1 + \sin^2 k_-).$$

Solving the corresponding to (2.22) equation for  $a^2$  gives the neutral stability curve for an arbitrary plane wave with  $|k_-| \in [0, \frac{\pi}{2}]$ . The analytical solution can be found by using Cardano's method, but is not written here for brevity. In the particular case  $k_- = 0$ , the neutral stability curve can be simply expressed as

$$(2.23) \quad a_M^2 = \frac{1}{4} \left( 3\alpha + \sqrt{\alpha^2 + 8C^2} \right),$$

which coincides with the result obtained in [43] for the ring of coupled oscillators without delay (and also for a ring with large delay). By substituting (2.9a) into (2.22), one can obtain the minimal  $\alpha = \alpha_0$  with

$$\alpha_0(k_-, k_\tau) = R \cos k_\tau \frac{1 - 2(\cos^2 k_- - \sin^2 k_\tau)}{\cos^2 k_- - \sin^2 k_\tau},$$

where a plane wave with particular  $k_-$  and  $k_\tau$  stabilizes.

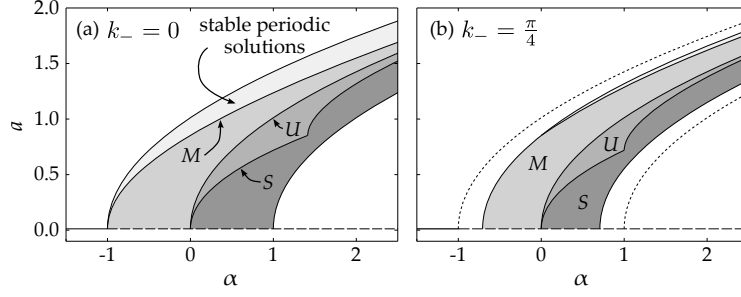


FIG. 2.5. Stability diagrams for periodic solutions of the SL-system (2.1) with different values of  $k_-$ : (a)  $k_- = 0$  and (b)  $k_- = \pi/4$ . The regime of stable periodic solutions is filled with a light gray and is located above the M-labeled curve in this projection. The curves denote the upper boundaries of the different stability regimes discussed in the text: M modulational instability, U uniform instability and S strong instability. The size of the stable regime decreases with the increasing of  $k_-$ .

The bifurcation diagram in Fig. 2.5 summarizes and illustrates the obtained results, showing the regions where the plane waves are stable (light gray), weakly unstable (darker gray, labeled with U and M), and strongly unstable (dark gray, labeled with S).

**2.2.4. Qualitative summary for the plane waves in coupled Stuart-Landau model.** The main qualitative conclusions of this relatively technical section are as follows: The family of plane wave solutions (2.8) is located on the circles (2.10) (for a fixed  $k_-$ ), and the number of plane waves grows accordingly to (2.11). The stability of a plane wave is governed by the characteristic equation (2.15) and determined by its position on the circle. More specifically, the plane waves with the higher amplitude tend to be more stable than those with the lower amplitude. Figure 2.5 illustrates this by showing stable, as well as weakly and strongly unstable “positions” on the circle. Thus, with the increasing  $\alpha$ , the number of stable plane waves increases. Plane waves with smaller  $|k_-|$  also tend to be more stable than those with larger  $|k_-|$ . Therefore we expect that the plane waves which are almost diagonal are more abundantly observed.

**3. FitzHugh-Nagumo neurons with homogeneous coupling delays.** In this section we consider a lattice of  $M \times N$  delay-coupled FitzHugh-Nagumo neurons, which are coupled via excitatory chemical synapses. The coupling architecture is the same as described in section 1. The model system reads

$$\begin{aligned}
 \frac{d}{dt}v_{m,n} &= v_{m,n} - \frac{1}{3}v_{m,n}^3 - w_{m,n} + I + \\
 &\quad + \frac{C}{2}(v_r - v_{m,n})(s_{m-1,n}(t - \tau) + s_{m,n-1}(t - \tau)) \\
 \frac{d}{dt}w_{m,n} &= \varepsilon(v_{m,n} + a - bw_{m,n}) \\
 \frac{d}{dt}s_{m,n} &= \alpha(v_{m,n})(1 - s_{m,n}) - 0.6s_{m,n}
 \end{aligned}
 \tag{3.1}$$

with  $\alpha(v) = \frac{1}{2}[1 + e^{-5(v-1)}]^{-1}$ . The variable  $v_{m,n}$  denotes the membrane potential of the corresponding neuron and  $w_{m,n}$  is a recovery variable, combining several microscopic dynamical variables of the biological neuron. The external stimulus current applied to the neuron is denoted by  $I$  and  $C$  is the coupling strength. We fix the

parameters  $a = 0.7$ ,  $b = 0.8$ , and  $\varepsilon = 0.08$ . The reversal potential is taken as  $v_r = 2$  for excitatory coupling. Similar model equations have been investigated in [26, 42] for unidirectional rings.

We demonstrate that the destabilization of the homogeneous steady state, the set of plane waves as well as their stability properties possess the same qualitative features which we observed in the previous section on Stuart-Landau oscillators. However, the apparent difficulty for the analysis of nonlinear plane waves is that they are not known analytically. Therefore we use numerical bifurcation analysis with DDE-BIFTOOL [9] and have to restrict ourselves to relatively small lattice size and delay values in Sec. 3.2.

**3.1. Homogeneous steady state and its stability.** The system (3.1) has a homogeneous steady state  $\bar{\mathbf{u}} = (\bar{v}, \bar{w}, \bar{s})$ . The value for the membrane resting potential  $\bar{v}$  can be obtained as a solution of the scalar equation

$$(3.2) \quad 0 = \bar{v} - \frac{1}{3}\bar{v}^3 - \frac{\bar{v} + a}{b} + I + C(v_r - \bar{v}) \frac{\alpha(\bar{v})}{\alpha(\bar{v}) + 0.6}.$$

The steady-state values of the remaining variables follow as

$$\bar{w} = \frac{\bar{v} + a}{b}, \quad \text{and} \quad \bar{s} = \frac{\alpha(\bar{v})}{\alpha(\bar{v}) + 0.6}.$$

In the case of weak coupling strength the homogeneous stationary state is unique, but for  $C_{\text{SN}} = 1.46475$  a saddle-node bifurcation of the equilibrium takes place. For strong coupling  $C > C_{\text{SN}}$  there is a domain of the control parameter  $I$  with three coexisting stationary states, see Fig. 3.1. In order to analyze the stability of the stationary state, we derive the linearized evolution equation for small perturbations of the equilibrium and subsequently diagonalize it in Fourier-space, just as in the previous section. One obtains the system

$$\frac{d}{dt} \delta \tilde{\mathbf{u}}(t) = A \delta \tilde{\mathbf{u}}(t) + 2B \cos(k_-) e^{ik_+} \delta \tilde{\mathbf{u}}(t - \tau)$$

with the real valued matrices

$$A = \begin{pmatrix} 1 - \bar{v}^2 - C\bar{s} & -1 & 0 \\ \varepsilon & -b\varepsilon & 0 \\ 5\alpha(\bar{v})(1 - 2\alpha(\bar{v}))(1 - \bar{s}) & 0 & -\alpha(\bar{v}) - 0.6 \end{pmatrix}$$

and

$$B = \begin{pmatrix} 0 & 0 & \frac{C}{2}(v_r - \bar{v}) \\ 0 & 0 & 0 \\ 0 & 0 & 0 \end{pmatrix}.$$

The corresponding characteristic equation reads

$$(3.3) \quad 0 = \prod_{\{(k_+, k_-)\}} \det | -\lambda \text{Id} + A + 2B \cos(k_-) e^{ik_+} e^{-\lambda\tau} |,$$

where Id represents the  $3 \times 3$  identity matrix. Similarly to the previous analysis, the stability of the homogeneous steady state is completely determined by the Eq. (3.3), which can be studied numerically using e.g. Newton-Raphson iteration. An additional insight in the properties of the spectrum can be given using the large delay approximation, which is done in Sec 3.1.1. Further, in Sec. 3.2, we study the appearance of periodic solutions in Hopf bifurcations.

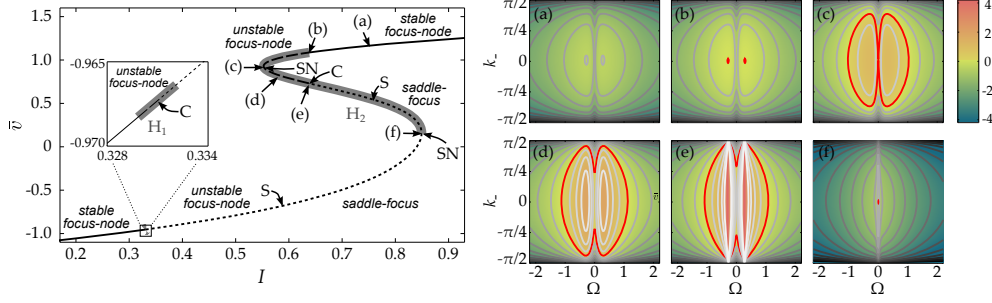


FIG. 3.1. Homogeneous stationary state and its bifurcations for  $C = 3$  for the FitzHugh-Nagumo model Eq. (3.1). In the case of an infinitely large lattice, the spectrum is described by the hybrid dispersion relation (3.4), parametrized by two continuous parameters  $\Omega$  and  $k_-$ , shown on the right. The color denotes the real parts of the eigenvalues: (a) stable stationary state, (b) destabilization via Hopf-bifurcation, (c) saddle-node bifurcation (SN), where an eigenvalue with  $\Omega = 0$  becomes unstable, (d) weakly unstable stationary state, (e) cusp bifurcation (C) and appearance of a strongly unstable spectrum, (f) saddle-node bifurcation and lower boundary of the Hopf-domain  $H_2$ .

### 3.1.1. Large delay approximation.

**Strongly unstable spectrum.** The strongly unstable spectrum results from considering only the instantaneous part of Eq. (3.3)

$$0 = \det |A - \lambda \text{Id}| = (a_{33} - \lambda) [(a_{11} - \lambda)(a_{22} - \lambda) - a_{21}a_{12}].$$

There is always one real solution  $\lambda_0 = a_{33} \leq -0.6$  of this 3rd-order polynomial, which is strictly negative. The remaining eigenvalues are

$$\lambda_{\pm} = \frac{1}{2} \left( a_{11} - b\varepsilon \pm \sqrt{(a_{11} + b\varepsilon)^2 - 4\varepsilon} \right).$$

Note that all relevant parameters are contained in  $a_{11} = 1 - \bar{v}^2 - C\bar{s}$ , involving the current  $I$  and coupling strength  $C$  directly or via the corresponding homogeneous steady state, respectively.

The strongly unstable spectrum exists when the real part of the largest eigenvalue  $\lambda_+$  is positive. This is the case when  $a_{11} > b\varepsilon$ . The appearance of the strongly unstable spectrum occurs at the cusp-bifurcation of the asymptotic continuous spectrum and labeled as ‘‘C’’ in Fig. 3.1. Moreover, there exists a pair of complex conjugate eigenvalues for  $a_{11} < 2\sqrt{\varepsilon} - b\varepsilon$ , otherwise the eigenvalues are real. The corresponding boundary is labeled with ‘‘S’’ in Fig. 3.1 and mediates the transition between an unstable focus-node and a saddle-focus.

**Pseudo-continuous spectrum.** The primary bifurcations of the steady state are captured by the pseudo-continuous spectrum. Just as in the previous section in the case of Stuart-Landau oscillators, this can be found by applying the ansatz  $\lambda = \gamma/\tau + i\Omega$ . Neglecting terms of order  $\mathcal{O}(1/\tau)$  and introducing the variable  $Y = e^{-\gamma} e^{i(k_+ - \Omega\tau)}$  yields the modified characteristic equation

$$\begin{aligned} 0 = \det |-i\Omega \text{Id} + A + 2B \cos k_- Y| &= \det \begin{vmatrix} a_{11} - i\Omega & a_{12} & 2b_{13} \cos k_- Y \\ a_{21} & a_{22} - i\Omega & 0 \\ a_{31} & 0 & a_{33} - i\Omega \end{vmatrix} = \\ &= (a_{11} - i\Omega)(a_{22} - i\Omega)(a_{33} - i\Omega) - 2(a_{22} - i\Omega)a_{31}b_{13} \cos k_- Y - (a_{33} - i\Omega)a_{12}a_{21}. \end{aligned}$$

Due to the simple linear coupling-structure, this is a linear equation in  $Y$ , which can be solved as

$$Y = \frac{a_{33} - i\Omega}{2a_{31}b_{13} \cos k_-} \left( a_{11} - i\Omega - \frac{a_{12}a_{21}}{a_{22} - i\Omega} \right),$$

leading to the asymptotic continuous spectrum

$$(3.4) \quad \gamma(\Omega, k_-) = -\log |Y(\Omega, k_-)|$$

This is a function of two parameters, determining the spectrum and stability of the steady state with respect to the perturbations with the spatial mode  $k_-$  (and independent on  $k_+$ ) and the delay-induced temporal modes  $\Omega$ . Some plots of this surface are illustrated in Fig. 3.1. Apparently the destabilization is similar to the case of Stuart-Landau oscillators described in Sec. 2.1.2. The asymptotic weak spectrum is invariant with respect to  $\Omega \rightarrow -\Omega$ ,  $k_- \rightarrow -k_-$  and  $k_- \rightarrow k_- + n\pi$ ,  $n \in \mathbb{Z}$ . The bifurcations of (3.4) lead to the boundaries of domains, where Hopf bifurcations are possible (shown as  $H_1$  and  $H_2$  in Fig. 3.1), and saddle-node-bifurcations. Many properties (such as extrema and roots) of the hybrid dispersion relation (3.4) are analytically accessible, but not given here explicitly, since they involve solutions of 3rd order polynomials.

**3.2. Hopf bifurcations and periodic attractors.** The Hopf bifurcations of the stationary state can be computed by setting  $\lambda = i\Omega$  in Eq. (3.3) and subsequently separating the resulting complex equation into two real equations. Using  $\bar{v}$  and  $\omega$  as parameters, the system can be solved by using e.g. Newton-Raphson iterations. The corresponding value of the bifurcation-parameter  $I$  follows uniquely from Eq. (3.2). Using the software package DDE-BIFTOOL [9], we perform a continuation of the Hopf bifurcations in the  $(I, \tau)$ -plane. The result is shown in Fig. 3.2, where the Hopf frequency  $\Omega$  is plotted vs. the time delay  $\tau$ . The structure of the branches can be understood by using reappearance arguments for periodic solutions [41]. Some of the Hopf branches terminate with zero frequency in a homoclinic bifurcation.

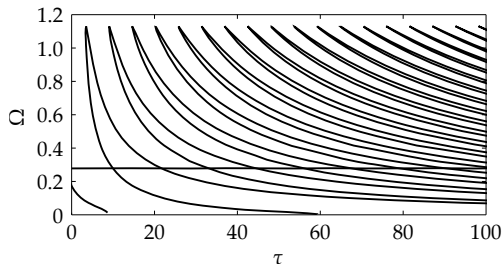


FIG. 3.2. Hopf bifurcation branches of a single FHN oscillator with delayed feedback with  $C = 3$ . For  $M \times N$  lattices similar structures can be obtained. The parameters used are given in the text.

Using DDE-BIFTOOL, we perform a numerical continuation of the periodic solutions, emerging from the Hopf bifurcations. The spatial orientation of a periodic solution is conserved along the branch, while varying the external current  $I$  as a control parameter. Typically, a periodic solution connects two Hopf points, which are both solutions of Eq. (3.3) with the same  $k_+$  and  $k_-$ . For vanishing delay, all stable periodic orbits are diagonal travelling waves with  $k_- = 0$ , including the synchronized solution. Increasing the coupling delay significantly enhances the stability properties

of periodic solutions and allows for stable travelling waves with  $k_- \neq 0$ . Moreover, the periodic solutions appear in a larger regime of the control parameter  $I$ . Snapshots of several coexisting travelling waves in a system of  $100 \times 100$  FHN-neurons with  $\tau = 50$  are shown in Fig. 3.4. Such solutions serve as the starting point for the more complicated patterns in systems with inhomogeneous delays, discussed in the following section.

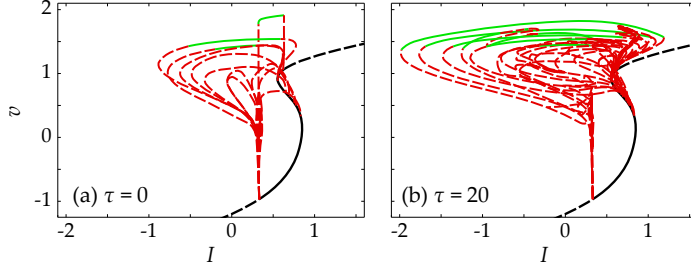


FIG. 3.3. Bifurcation diagrams for  $3 \times 3$ -lattices of coupled FHN neurons with  $C = 3$  and different delays: (a)  $\tau = 0$  and (b)  $\tau = 20$ . Green solid lines denote stable periodic solutions, red dashed lines show unstable ones. The stable stationary state is depicted by a black solid line, unstable steady states by a black dashed line. The parameters used are given in the text.

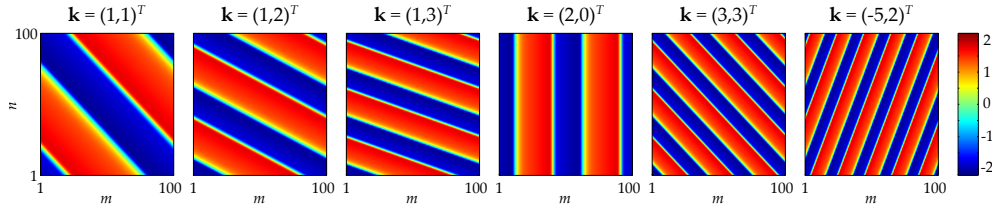


FIG. 3.4. Snapshots of several coexisting stable travelling waves in a  $100 \times 100$ -lattice of delay-coupled FHN neurons with  $C = 3$ ,  $I = 0$  and  $\tau = 50$ . The color denotes the value of the membrane voltage  $v_{m,n}$  of the corresponding neuron.

#### 4. Patterns in systems with inhomogeneous delays.

**4.1. Componentwise time-shift transformation.** Consider a delayed dynamical system with a coupling topology as described by Eq. (1.1) with homogeneous delays. As follows from the previous analysis, for sufficiently large delay  $\tau$  the homogeneous system possesses a large set of stable plane waves, including stable spatially homogeneous time-periodic solutions.

We can transform the plane waves of the homogeneous system into an (almost) arbitrary pattern by adjusting the coupling delays. The derivation of the transformation presented here is a generalization of the method described in [28, 42] for unidirectionally coupled rings and [22] for arbitrary networks with delays.

Rewriting the system (1.1) with homogeneous delays  $\tau$  with respect to the new coordinates  $\mathbf{v}$  given by  $\mathbf{u}_{m,n}(t) = \mathbf{v}_{m,n}(t - \eta_{m,n})$  leads to the system

$$\begin{aligned} \dot{\mathbf{v}}_{m,n}(t) &= \mathbf{F}(\mathbf{v}_{m,n}(t), \mathbf{v}_{m-1,n}(t + \eta_{m,n} - \eta_{m-1,n} - \tau) + \\ &\quad + \mathbf{v}_{m,n-1}(t + \eta_{m,n} - \eta_{m,n-1} - \tau)) \\ &= \mathbf{F}(\mathbf{v}_{m,n}(t), \mathbf{v}_{m-1,n}(t - \tau_{m,n}^{\downarrow}) + \mathbf{v}_{m,n-1}(t - \tau_{m,n}^{\rightarrow})) \end{aligned}$$

with adjusted non-homogeneous delays

$$(4.1) \quad \begin{aligned} \tau_{m,n}^{\downarrow} &= \tau - \eta_{m,n} + \eta_{m-1,n}, \\ \tau_{m,n}^{\rightarrow} &= \tau - \eta_{m,n} + \eta_{m,n-1}. \end{aligned}$$

The timeshifts  $\eta \in \mathbb{R}^{M \times N}$  can have an arbitrary form, up to the restriction that the new delays need to be positive. By adjusting the timeshifts, one can obtain stable, time-periodic attractors of various spatial forms. For example, a stable synchronous periodic solution  $\mathbf{u}_{m,n}(t) = \mathbf{u}_0(t) = \mathbf{u}_0(t+T)$  of the homogeneous system corresponds to a solution  $\mathbf{v}_{m,n}(t) = \mathbf{u}_0(t + \eta_{m,n})$  of the non-homogeneous system, where each component is shifted in time by an amount  $\eta_{m,n}$ . According to [21, 22], the stability properties of the periodic solutions are kept by the transformation. This shift will result to a shifted value of the dynamical variables (e.g. voltage for the neuronal models). Thus, the encoded pattern  $\eta_{m,n}$  will be visible in the dynamical variables. Since  $\eta_{m,n}$  is practically arbitrary, there is a variety of patterns, which can appear as stable attractors in the systems with inhomogeneously delayed connections.

**4.2. Examples.** Some illustrative examples for stable spatio-temporal patterns in a lattice with non-homogeneous delays are shown in Figs. 1.2, 4.1, and 4.2. All examples are constructed from synchronized solutions with  $\mathbf{k} = (0,0)^T$  via the delay-transformation (4.1). However, the scaling of the patterns  $\eta_{m,n}$  with respect to the period time is different in the examples. In the ‘‘Mona Lisa’’-pattern (Fig. 1.2) the spiking times are chosen only slightly different, so that the pattern is a slightly adapted standing front solution. In the examples in Fig. 4.1 and 4.2 the spiking-times are distributed over the whole period.

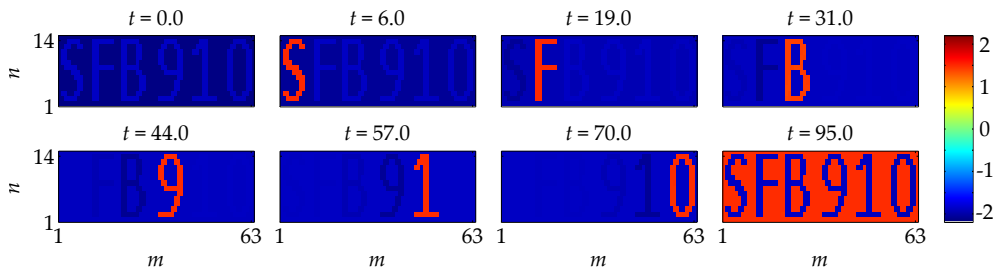


FIG. 4.1. Snapshots of the ‘‘SFB 910’’-pattern in a  $63 \times 14$ -lattice of delay-coupled FHN-neurons with  $C = 3$  and  $I = -2$ . There are several clusters of neurons, spiking synchronously. The pattern oscillates with a period  $T = 102.3$ .

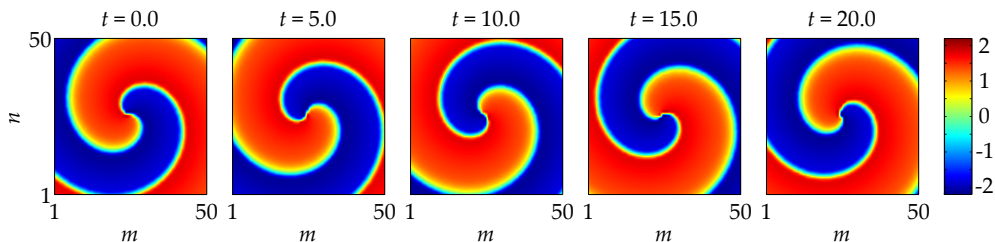


FIG. 4.2. Snapshots of a spiral wave pattern in a  $50 \times 50$ -lattice of delay-coupled FHN-neurons with  $C = 3$  and  $I = 0$ . The pattern periodically reappears with a period  $T = 25.8$ .

**5. Conclusions.** The linear stability of time-periodic patterns has been studied analytically in the limit of large delay in terms of a hybrid dispersion relation.

We have shown that arbitrary stable spatio-temporal periodic patterns can be created in two-dimensional lattices of coupled oscillators with inhomogeneous coupling delays. We propose that this offers interesting applications for the generation, storage, and information processing of visual patterns, for instance in networks of optoelectronic [36] or electronic [30] oscillators. Our results have been illustrated with two models of the local node dynamics which have a wide range of applicability: (i) the Stuart-Landau oscillator, i.e., a generic model which arises by center-manifold expansion of a limit cycle system near a supercritical Hopf bifurcation, and (ii) the FitzHugh-Nagumo model, which is a generic model of neuronal spiking dynamics.

**Acknowledgements.** We thank L. Lücken and M. Zaks for useful discussions and the DFG for financial support in the framework of the Collaborative Research Center SFB 910.

#### REFERENCES

- [1] S. BUNGAY AND S. CAMPBELL, *Patterns of oscillation in a ring of identical cells with delayed coupling*, Int. J. Bifurcation and Chaos, 17 (2007), pp. 3109 – 3125.
- [2] E. S. C. CAKAN, J. LEHNERT, *Heterogeneous delays in neural networks*, Eur. Phys. J. B, (2014). arXiv:1311.1919v1.
- [3] S. A. CAMPBELL, *Time delays in neural systems*, in Handbook of brain connectivity, Springer, 2007, pp. 65–90.
- [4] C. U. CHOE, R.-S. KIM, H. JANG, P. HÖVEL, AND E. SCHÖLL, *Delayed-feedback control with arbitrary and distributed delay-time and noninvasive control of synchrony in networks coupled with heterogeneous delays*, Int. J. Dynam. Control, (2014). In print.
- [5] M. CROSS AND H. GREENSIDE, *Pattern Formation and Dynamics in Nonequilibrium Systems*, Cambridge University Press, Cambridge, 2009.
- [6] M. C. CROSS AND P. C. HOHENBERG, *Pattern formation outside of equilibrium*, Rev. Mod. Phys., 65 (1993), pp. 851 – 1112.
- [7] T. DAHMS, J. LEHNERT, AND E. SCHÖLL, *Cluster and group synchronization in delay-coupled networks*, Phys. Rev. E, 86 (2012), p. 016202.
- [8] O. D’HUYSS, S. ZEEB, T. JÜNGLING, S. HEILGENTHAL, S. YANCHUK, AND W. KINZEL, *Synchronisation and scaling properties of chaotic networks with multiple delays*, EPL (Europhysics Letters), 103 (2013), p. 10013.
- [9] K. ENGELBORGH, T. LUZYANINA, AND D. ROOSE, *Numerical bifurcation analysis of delay differential equations using dde-biftool*, ACM Trans. Math. Software, 28 (2002), pp. 1–21.
- [10] B. FIEDLER, V. FLUNKERT, M. GEORGI, P. HOVEL, AND E. SCHÖLL, *Refuting the odd-number limitation of time-delayed feedback control*, Phys. Rev. Lett., 98 (2007), p. 114101.
- [11] R. FITZHUGH, *Impulses and physiological states in theoretical models of nerve membrane*, Biophys. J., 1 (1961), pp. 445–466.
- [12] V. FLUNKERT, I. FISCHER, AND E. SCHÖLL, *Dynamics, control and information in delay-coupled systems*, Philosophical Transactions of the Royal Society A: Mathematical, Physical and Engineering Sciences Physical and Engineering Sciences, 371 (2013), p. 20120465.
- [13] V. FLUNKERT, S. YANCHUK, T. DAHMS, AND E. SCHÖLL, *Synchronizing distant nodes: A universal classification of networks*, Phys. Rev. Lett., 105 (2010), p. 254101.
- [14] A. L. FRANZ, R. ROY, L. B. SHAW, AND I. B. SCHWARTZ, *Effect of multiple time delays on intensity fluctuation dynamics in fiber ring lasers*, Phys. Rev. E, 78 (2008), p. 016208.
- [15] G. GIACOMELLI, F. MARINO, M. A. ZAKS, AND S. YANCHUK, *Coarsening in a bistable system with long-delayed feedback*, EPL (Europhysics Letters), 99 (2012), p. 58005.
- [16] E. M. IZHKEVICH, *Polychronization: Computation with spikes*, Neural Computation, 18 (2006), pp. 245–282.
- [17] W. JUST, A. PELSTER, M. SCHANZ, AND E. SCHÖLL, *Delayed complex systems*, Phil. Trans. Roy. Soc. A, 368 (2010), pp. 301–513.
- [18] W. KINZEL, A. ENGLERT, G. REENTS, M. ZIGZAG, AND I. KANTER, *Synchronization of networks of chaotic units with time-delayed couplings*, Phys. Rev. E, 79 (2009), p. 056207.

- [19] L. LARGER, B. PENKOVSKY, AND Y. MAISTRENKO, *Virtual chimera states for delayed-feedback systems*, Phys. Rev. Lett., 111 (2013), p. 054103.
- [20] M. LICHTNER, M. WOLFRUM, AND S. YANCHUK, *The spectrum of delay differential equations with large delay*, SIAM J. Math. Anal., 43 (2011), pp. 788–802.
- [21] L. LÜCKEN, J. P. PADE, K. KNAUER, AND S. YANCHUK, *Parameter space dimension for networks with transmission delays*. arXiv:1301.2051, Jan. 2013.
- [22] L. LÜCKEN, J. P. PADE, AND S. YANCHUK, *Reduction of interaction delays in networks*, EPL (Europhysics Letters), 103 (2013), p. 10006.
- [23] K. LÜDGE, ed., *Nonlinear Laser Dynamics: From Quantum Dots to Cryptography*, Wiley-VCH, 2012.
- [24] J. NAGUMO, S. ARIMOTO, AND S. YOSHIKAWA, *An active pulse transmission line simulating nerve axon*, Proc. IRE, (1962), pp. 2061–2071.
- [25] G. OROSZ, R. E. WILSON, AND G. STEPAN, *Traffic jams: dynamics and control*, Phil. Trans. R. Soc. A, 368 (2010), pp. 4455–4479.
- [26] P. PERLIKOWSKI, S. YANCHUK, O. V. POPOVYCH, AND P. A. TASS, *Periodic patterns in a ring of delay-coupled oscillators*, Phys. Rev. E, 82 (2010), p. 036208.
- [27] D. PIEROUX AND P. MANDEL, *Low-frequency fluctuations in the lang-kobayashi equations*, Phys. Rev. E, 68 (2003).
- [28] O. V. POPOVYCH, S. YANCHUK, AND P. A. TASS, *Delay- and coupling-induced firing patterns in oscillatory neural loops*, Phys. Rev. Lett., 107 (2011), p. 228102.
- [29] D. V. RAMANA REDDY, A. SEN, AND G. L. JOHNSTON, *Experimental evidence of time-delay-induced death in coupled limit-cycle oscillators*, Phys. Rev. Lett., 85 (2000), pp. 3381–3384.
- [30] D. P. ROSIN, D. RONTANI, D. J. GAUTHIER, AND E. SCHÖLL, *Control of synchronization patterns in neural-like boolean networks*, Phys. Rev. Lett., 110 (2013), p. 104102.
- [31] J. SIEBER, M. WOLFRUM, M. LICHTNER, AND S. YANCHUK, *On the stability of periodic orbits in delay equations with large delay*, Discrete Contin. Dyn. Syst. A, 33 (2013), pp. 3109–3134.
- [32] M. C. SORIANO, J. GARCÍA-OJALVO, C. R. MIRASSO, AND I. FISCHER, *Complex photonics: Dynamics and applications of delay-coupled semiconductor lasers*, Rev. Mod. Phys., 85 (2013), pp. 421–470.
- [33] G. STEPAN, *Delay effects in brain dynamics*, Phil. Trans. Roy. Soc. A, 367 (2009), pp. 1059–1062.
- [34] R. SZALAI AND G. OROSZ, *Decomposing the dynamics of heterogeneous delayed networks with applications to connected vehicle systems*, Phys. Rev. E, 88 (2013), p. 040902.
- [35] G. TIANA AND M. H. JENSEN, *The dynamics of genetic control in the cell: the good and bad of being late*, Phil. Trans. Roy. Soc. A, 371 (2013).
- [36] C. R. S. WILLIAMS, T. E. MURPHY, R. ROY, F. SORRENTINO, T. DAHMS, AND E. SCHÖLL, *Experimental observations of group synchrony in a system of chaotic optoelectronic oscillators*, Phys. Rev. Lett., 110 (2013), p. 064104.
- [37] C. R. S. WILLIAMS, F. SORRENTINO, T. E. MURPHY, AND R. ROY, *Synchronization states and multistability in a ring of periodic oscillators: Experimentally variable coupling delays*, Chaos, 23 (2013).
- [38] M. WOLFRUM AND S. YANCHUK, *Eckhaus instability in systems with large delay*, Phys. Rev. Lett., 96 (2006), p. 220201.
- [39] M. WOLFRUM, S. YANCHUK, P. HÖVEL, AND E. SCHÖLL, *Complex dynamics in delay-differential equations with large delay*, Eur. Phys. J. Special Topics, 191 (2010), pp. 91–103.
- [40] S. YANCHUK, *Properties of stationary states of delay equations with large delay and applications to laser dynamics*, Math. Methods Appl. Sci., 28 (2005), pp. 363–377.
- [41] S. YANCHUK AND P. PERLIKOWSKI, *Delay and periodicity*, Phys. Rev. E, 79 (2009), p. 046221.
- [42] S. YANCHUK, P. PERLIKOWSKI, O. V. POPOVYCH, AND P. A. TASS, *Variability of spatio-temporal patterns in non-homogeneous rings of spiking neurons.*, Chaos, 21 (2011), p. 047511.
- [43] S. YANCHUK AND M. WOLFRUM, *Destabilization patterns in chains of coupled oscillators*, Phys. Rev. E, 77 (2008), p. 026212.
- [44] A. ZAKHAROVA, I. SCHNEIDER, Y. N. KYRYCHKO, K. B. BLYUSS, A. KOSKESKA, B. FIEDLER, AND E. SCHÖLL, *Time delay control of symmetry-breaking primary and secondary oscillation death*, EPL (Europhysics Letters), 104 (2013), p. 50004.